Feasibility study on 3-D shape analysis of high-aspect-ratio features using through-focus scanning optical microscopy

Ravi Kiran Attota,[1*] Peter Weck,[2] John A. Kramar,[1] Benjamin Bunday[3] and Victor Vartanian[3]

[1]Engineering Physics Division, PML, NIST, Gaithersburg, MD 20899, USA
[2]Swarthmore College, 500 College Ave., Swarthmore, PA 19081, USA
[3]SUNY Politechnic SEMATECH, 257 Fuller Road, Suite 2200, Albany, NY, 12203, USA
[*]ravikiran.attota@nist.gov

Abstract: In-line metrologies currently used in the semiconductor industry are being challenged by the aggressive pace of device scaling and the adoption of novel device architectures. Metrology and process control of three-dimensional (3-D) high-aspect-ratio (HAR) features are becoming increasingly important and also challenging. In this paper we present a feasibility study of through-focus scanning optical microscopy (TSOM) for 3-D shape analysis of HAR features. TSOM makes use of 3-D optical data collected using a conventional optical microscope for 3-D shape analysis. Simulation results of trenches and holes down to the 11 nm node are presented. The ability of TSOM to analyze an array of HAR features or a single isolated HAR feature is also presented. This allows for the use of targets with area over 100 times smaller than that of conventional gratings, saving valuable real estate on the wafers. Indications are that the sensitivity of TSOM may match or exceed the International Technology Roadmap for Semiconductors (ITRS) measurement requirements for the next several years. Both simulations and preliminary experimental results are presented. The simplicity, lowcost, high throughput, and nanometer scale 3-D shape sensitivity of TSOM make it an attractive inspection and process monitoring solution for nanomanufacturing.

OCIS codes: (120.0120) Instrumentation, measurement, and metrology; (120.3930) Metrological instrumentation; (180.5810) Scanning microscopy; (180.6900) Three-dimensional microscopy.

References and links

1. J. Vila-Comamala, S. Gorelick, V. A. Guzenko, E. Farm, M. Ritala, and C. David, "Dense high aspect ratio hydrogen silsesquioxane nanostructures by 100 keV electron beam lithography," Nanotechnology **21**, 285305 (2010).
2. C. Chang and A. Sakdinawat, "Ultra-high aspect ratio high-resolution nanofabrication for hard X-ray diffractive optics," Nat. Commun. **5**, 4243 (2014).
3. B. Bunday, T. A. Germer, V. Vartanian, A. Cordes, A. Cepler, and C. Settens, "Gaps analysis for CD metrology beyond the 22 nm node," Proc. SPIE **8681**, 86813B (2013).
4. T. M. Bao, Y. Bar, D. Fong, and M. Godbole, "Improving dry etch control for contact plugs in advanced DRAM manufacturing," Proc. SPIE **6922**, 69223G (2008).
5. A. W. Topol, D. C. L. Tulipe, L. Shi, D. J. Frank, K. Bernstein, S. E. Steen, A. Kumar, G. U. Singco, A. M. Young, K. W. Guarini, and M. Ieong, "Three-dimensional integrated circuits," IBM Journal of Research and Development 50, 491-506 (2006).
6. Y. S. Ku, D. M. Shyu, P. Y. Chang, and W. T. Hsu, "In-line metrology of 3D interconnect processes," Proc. SPIE **8324**, 832411 (2012).
7. O. Fursenko, J. Bauer, S. Marschmeyer, and H. P. Stoll, "Through silicon via profile metrology of Bosch etching process based on spectroscopic reflectometry," Microelectron Eng. 139, 70-75 (2015).

8. M. Nakamura, H. Kitada, and S. Sakuyama, "Direct depth measurement tool of high aspect ratio via-hole for three-dimensional stacked devices," J. Surface Analysis **20**, 182-186 (2014).
9. K. Takamasu, Y. Iwaki, S. Takahashi, H. Kawada, M. Ikota, G. F. Lorusso, and N. Horiguchi, "3D-profile measurement of advanced semiconductor features by reference metrology," Proc. SPIE **9778**, 97781T (2016).
10. I. Schulmeyer, L. Lechner, A. Gu, R. Estrada, D. Stewart, L. Stern, S. McVey, B. Goetze, U. Mantz, and R. Jammy, "Advanced metrology and inspection solutions for a 3D world," Proc. 2016 International Symposium on VLSI Technology, Systems and Application (VLSI-TSA), 1-2 (2016).
11. A. J. Cepler, B. Bunday, B. L. Thiel, and J. S. Villarrubia, "Scanning electron microscopy imaging of ultra-high aspect ratio hole features," Proc. SPIE **8324,** 83241N **(**2012).
12. A. Arceo, B. Bunday, A. Cordes, and V. Vartanian, "Evolution or revolution: the path for metrology beyond the 22nm node," Solid State Technol **55**, 15-19 (2012).
13. R. K. Leach, R. Boyd, T. Burke, H. U. Danzebrink, K. Dirscherl, T. Dziomba, M. Gee, L. Koenders, V. Morazzani, A. Pidduck, D. Roy, W. E. S. Unger, and A. Yacoot, "The European nanometrology landscape," Nanotechnology **22**, 062001 (2011).
14. R. A. Allen, V. Vartanian, D. Read, and W. Baylies, "(Invited) Metrology for 3D Integration," Ecs Transactions **61**, 105-112 (2014).
15. T. M. Bao, L. Mininni, and D. Dawson, "Improving sidewall profile metrology with enhanced 3D-AFM," Lithography Asia 2008, 7140 (2008).
16. M. Caldwell, T. M. Bao, J. Hackenberg, B. McLain, O. Munoz, T. Stephens, and V. Vartanian, "Improved dimension and shape metrology with versatile atomic force microscopy," Proc. SPIE **6518**, 65181L (2007).
17. W. Hassler-Grohne, D. Huser, K. P. Johnsen, C. G. Frase, and H. Bosse, "Current limitations of SEM and AFM metrology for the characterization of 3D nanostructures," Meas. Sci. Technol **22**, 094003 (2011).
18. Y. S. Ku, "Spectral reflectometry for metrology of three-dimensional through-silicon vias," J Micro-Nanolith Mem. **13**, 011209 (2014).
19. X. X. Zhang, P. Snow, A. Vaid, E. Solecky, H. Zhou, Z. H. Ge, S. Yasharzade, O. Shoval, O. Adan, I. Schwarzband, and M. Bar-Zvi, "Solving next generation (1X node) metrology challenges using advanced CDSEM capabilities: tilt, high energy and backscatter imaging," Proc. SPIE **9424**, 94240G (2015).
20. V. Vartanian, R. A. Allen, L. Smith, K. Hummler, S. Olson, and B. Sapp, "Metrology needs for through-silicon via fabrication," MOEMS 13, 011206-011206 (2014).
21. S. I. Association, "The International Technology Roadmap for Semiconductors (ITRS) " (Semiconductor Industry Association, San Jose, 2011).
22. B. Bunday, "HVM metrology challenges towards the 5nm node," Proc. SPIE **9778**, 97780E (2016).
23. R. Attota, T. A. Germer, and R. M. Silver, "Through-focus scanning-optical-microscope imaging method for nanoscale dimensional analysis," Opt. Lett. **33**, 1990-1992 (2008).
24. R. Attota, R. G. Dixson, J. A. Kramar, J. E. Potzick, A. E. Vladar, B. Bunday, E. Novak, and A. Rudack, "TSOM method for semiconductor metrology," Proc. SPIE **7971**, 79710T (2011).
25. R. Attota and R. G. Dixson, "Resolving three-dimensional shape of sub-50 nm wide lines with nanometer-scale sensitivity using conventional optical microscopes," Appl. Phys. Lett. **105**, 043101 (2014).
26. M. Ryabko, Koptyev, S., Shchekin, A., Medvedev, A., "Improved critical dimension inspection for the semiconductor industry," SPIE Newsroom (2014).
27. M. Ryabko, S. Koptyaev, A. Shcherbakov, A. Lantsov, and S. Y. Oh, "Motion-free all optical inspection system for nanoscale topology control," Opt. Express **22**, 14958–14963 (2014).
28. M. Ryabko, A. Shchekin, S. Koptyaev, A. Lantsov, A. Medvedev, A. Shcherbakov, and S. Y. Oh, "Throughfocus scanning optical microscopy (TSOM) considering optical aberrations: practical implementation," Opt. Exp. **23**, 32215–32221 (2015).
29. R. Attota and R. Silver, "Nanometrology using a through-focus scanning optical microscopy method," Meas. Sci. Technol. **22,** 024002 (2011).
30. H. Kang, R. Attota, V. Tondare, A. E. Vladár, and P. Kavuri, "A method to determine the number of nanoparticles in a cluster using conventional optical microscopes," Appl. Phys. Lett. **107**, 103106 (2015).
31. R. Attota, "Noise analysis for through-focus scanning optical microscopy," Opt. Lett. **41**, 745-748 (2016).
32. T. Pistor, V., "Electromagnetic simulation and modeling with applications in lithography," (University of California, Berkeley, 2001).
33. C. Hartig, D. Fischer, B. Schulz, A. Vaid, O. Adan, S. Levi, A. Ge, J. Zhou, M. Bar-Zvi, R. Enge, and U. Groh, "Material contrast based inline metrology - process verification and control using Back Scattered Electron Imaging on CD-SEM," Proc. SPIE **8681**, 868108 (2013).
34. A. J. Cepler, B. Bunday, B. L. Thiel, and J. S. Villarrubia, "Scanning electron microscopy imaging of ultra-high aspect ratio hole features," Proc. SPIE **8324**, 83241N (2012).
35. R. K. Attota and H. Kang, "Parameter optimization for through-focus scanning optical microscopy," Opt. Exp. **24**, 14915-14924 (2016).
36. R. Attota, P. P. Kavuri, H. Kang, R. Kasica, and L. Chen, "Nanoparticle size determination using optical microscopes," Appl. Phys. Lett. **105**, 163105 (2014).
37. J. M. Gineste, P. Macko, E. A. Patterson, and M. P. Whelan, "Three-dimensional automated nanoparticle tracking using Mie scattering in an optical microscope," J. of Microscopy **243**, 172-178 (2011).

1. Introduction

Dimensional metrology of high aspect ratio (HAR) features [1-11] will become more challenging as technology progresses, particularly in memory applications where designs are evolving from planar to vertical architectures with multi-level gates assembled in 3-D structures [3, 11-20]. The basic building blocks of these features are deep trenches and holes in oxide, silicon, or multiple alternating layers of oxide and silicon. Furthermore, memory device scaling is headed towards aspect ratios ranging from 30:1 to 60:1, implying depths from 0.5 μm to 2 μm at the 32 nm and 11 nm International Technology Roadmap for Semiconductors (ITRS) node [3, 21] lateral dimensions. For example, HAR contact holes may be 1 μm in depth and 30 nm in diameter, for an aspect ratio of approximately 30:1 at the 32 nm node. From the process control perspective, CD metrology entails control of top CD, bottom CD, profile, and detection of residues, which introduce a new set of gaps in metrology capability, since current non-destructive metrology techniques lack the sensitivity and resolution to characterize such features [22]. Moreover, the physics of these measurements are hindered by the extremely deep and geometrically confined volumes involved. Charged particle-based imaging techniques such as CD scanning electron microscopy (CD-SEM), and helium ion microscopy (HeIM) have sensitivity limitations arising from sidewall charging, as only a small fraction of scattered particles ultimately reaches the detector.

The limitations outlined above prompt the need for alternative non-destructive metrology methods that can achieve sensitivity at the nanoscale while maintaining throughput compatible with high volume manufacturing. In light of this, optical techniques are desirable. A recently developed optical method is through-focus scanning optical microscopy (TSOM). In this paper we explore the application of TSOM for 3-D shape analysis of HAR targets, especially as an inspection and process monitoring tool. TSOM is a measurement technique that has the potential to fulfill the requirements of a non-destructive, high-throughput method with sensitivity on the nanometer scale [23-30]. The low cost of TSOM makes it a potential candidate for measuring features in high-volume manufacturing. In this work, we performed a series of simulations to examine the usage of TSOM for HAR CD metrology, and demonstrate this method using a test HAR trench wafer.

2.TSOM

TSOM makes use of a conventional optical microscope equipped with a digital camera and a motorized focus stage, and consists of collecting optical images at a range of focus positions and combining them into a 3-D volume of optical information. Preserving all available optical information in this 3-D space (*x, y,* and focus position) allows for performing dimensional analysis of a sample by generating a 2-D TSOM image from any direction or location in the x-y plane as a function of focus position [23, 25, 29]. A differential TSOM (D-TSOM) image is a pixel-by-pixel difference between two TSOM images. Three of the several important properties of D-TSOM images [24, 29] are given below.

1. D-TSOM images are often distinct for different types of parameter changes
2. D-TSOM images are qualitatively similar for different magnitude changes in the same parameter
3. Optical content of a D-TSOM image is proportional to the magnitude of the dimensional differences

Property 1 means that the D-TSOM images can serve as a "fingerprint" for different types of parameter variations. Property 2 means variation in a given parameter will scale the magnitude of the D-TSOM image without significantly changing its shape. Property 3 provides the magnitude of the difference and can be quantified with an optical intensity range (OIR)

metric [25], which is the absolute optical range of the differential signal and is scaled by 100. In the current work, we make use of these three D-TSOM image characteristics to determine 3-D shape variations of HAR structures.

This work contains both experiments and simulations. It is important to understand the experimental noise threshold to understand the sensitivity limitations of the simulation results and to determine whether a simulated TSOM result from a feature dimension perturbation would be distinguishable from background noise. It was found that the noise OIR of less than one provides an experimental noise threshold limit for the subsequent simulations [31]. To experimentally detect a dimensional difference safely, it is desirable to have the OIR of a D-TSOM image greater than one.

3. TSOM for HAR metrology: results and discussion

3.1 Simulations

TSOM was evaluated to determine sensitivity to 3-D shape variations on HAR features using simulations. A commercially available optical simulation program that uses a finite-difference time-domain (FDTD) method for solving Maxwell's equations was used in the current study [32]. The program can simulate optical images of 3-D objects at different focus positions. An in-house developed software program converts the optical output into a 3-D optical data set and then extracts the TSOM images from that dataset passing through the location of interest (i.e., target) for further analysis.

The simulation work was performed on simple HAR trench and hole structures. The material stacks were HAR trenches and holes in Si oxide deposited on Si, and HAR trenches in Si. The goal of the simulations was to evaluate TSOM sensitivity to nanometer scale 3-D shape changes in structural parameters of the HAR features such as CD, sidewall angle, and feature depth. The aspect ratio of the features is 40:1 for both the 11 nm and 32 nm design rule (DR) CDs selected. Simulations were also done for a 100 nm wide trench HAR test grating target having a 1 μm pitch and a 10:1 aspect ratio. Table 1 summarizes all the structural and optical parameters used in this simulation study.

Table 1. Optical and structural parameters used in TSOM simulations for HAR features.

Wavelength (λ), nm	520	520	520
Polarization, Degrees	0	0	90
Illumination numerical aperture (INA)	0.2	0.2	0.25
Collection numerical aperture (CNA)	0.8	0.8	0.75
Design rule (DR)	11	32	
Bottom CD (BW), nm	8-10	22-30	100-102
Trench/Via height (HT), nm	360-370	1000-1010	1100-1105
Pitch (PT), nm	22	64	1000
Sidewall angle (SW), Degrees	89.2-90	89.2-90	89.5-90
Number of trenches/Vias	7	1,3,7	Inf.

The first task was to optimize the parametric conditions under which TSOM provides high sensitivity [Fig. 1]. The effect of polarization was studied for trenches. For a 5 nm difference in the CD, 0° illumination polarization (e-field perpendicular to the trenches) showed higher sensitivity compared to 90° (e-field parallel to the trenches) as shown in Figs. 1(a) and 1(b). For this reason, 0° illumination polarization was used for all the subsequent simulations. As the number of trenches increased from 1 to 7, the OIRs of the D-TSOM images (sensitivity) for the 5 nm difference in the CD increased from 4.3 to 162 [Figs. 1(b) to 1(d)], as the interaction volume increases. The HAR target with 7 lines exhibited the highest sensitivity among the

targets studied. Consequently, a 7-trench HAR target was used for subsequent trench target studies. For the hole simulations, an array of 9 holes across was used, with periodic boundary conditions (i.e., infinite array of holes) at the hole spacing in the other dimension.

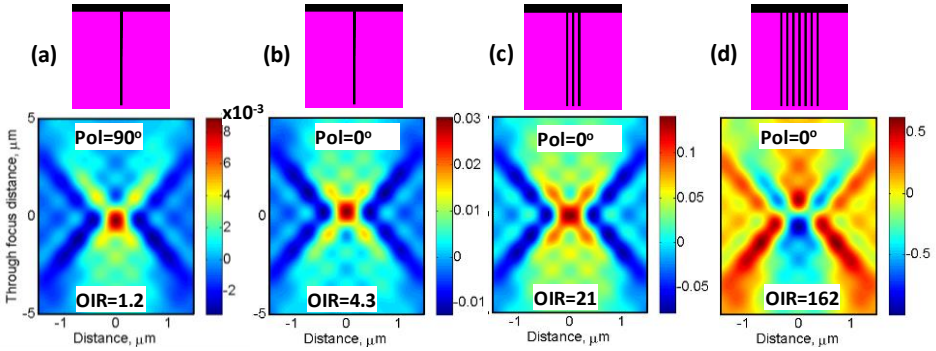

Fig.1. Selection of the optimized illumination polarization and the number of trenches, using HAR trenches in Si target as an example. Illumination polarization of 0o and increasing the number of trenches produce high sensitivity. Polarization state and OIR values are shown in the insets.

Trench/hole depth, sidewall angle, and bottom CD are some of the important parameters to monitor during fabrication. Therefore, variations in these parameters were studied for the parameter ranges shown in Table 1. Following industry requirements, trenches in Si and trenches and holes in oxide were studied [3]. The results for the 11 nm and 32 nm DR trench and hole structures are shown in Figs. 2 and 3. To arrive at the sensitivity threshold, each parameter was individually perturbed in small increments. D-TSOM images were evaluated at each new condition with reduced differences in parameters until the OIR was just above one.

Under the simulation conditions used, the overall TSOM sensitivity is similar for a 0.01˚ sidewall angle perturbation for all HAR targets studied for the two selected DRs. The CD parameter shows the best sensitivity: down to a 0.02 nm perturbation for 32 nm DR trenches. The worst CD sensitivity is 0.1 nm for 11 nm DR trenches in oxide. Depth sensitivity shows large variation among the two DRs studied, the smallest being 0.2 nm for 32 nm DR holes and the largest being 5 nm for 11 nm DR holes. This indicates strong dependence of depth sensitivity based on DR. A summary of potential TSOM sensitivities along with their percentage sensitivities is shown in Table. 2.

For trenches in Si, each depth, sidewall angle, and bottom CD variation resulted in dissimilar D-TSOM image patterns indicating that, in principle, these three parameters can be distinguished. However, for HAR trenches and holes in oxide, CD and sidewall differences show almost identical D-TSOM image patterns. Similarly, at a much lower illumination wavelength of 250 nm, HAR trenches and holes in oxide showed similar behavior when compared to 520 nm illumination (results not shown here). This indicates that TSOM property 1 seems to break in certain cases.

Simulation results indicate that TSOM potentially shows good sensitivity to sidewall angle variation, possibly better than other optical or CD-SEM metrology methods, with the ability to distinguish changes as small as 0.01˚ in both structures. For trenches, CD performance is in the same general range as scatterometry; however, TSOM measures isolated features or small arrays, whereas scatterometry measures dense features. CD-SEM as currently configured has more limitations with trenches for CD measurements, although it is reported that low-loss backscattering (LL-BSE) configurations can be used to image similar HAR features, with results in the same range as above [33]. As for depth sensitivity, scatterometery is predicted to be marginally better than the values shown above for TSOM simulations. CD-SEM in its current form is insensitive to depth [3]. Model base infrared (MBIR) optical measurement

appears to be similarly sensitive for dimensional variations, but needs an array of targets. It also needs further study to confirm its sensitivity as shown in a comprehensive comparative study of different metrology methods [22].

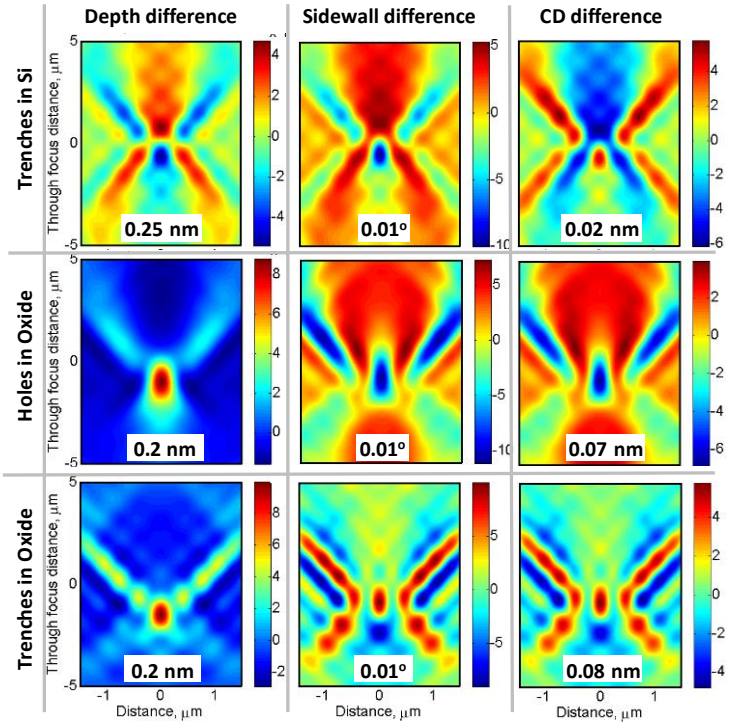

Fig. 2. Simulated D-TSOM images of 32 nm DR HAR trenches and holes showing minimum sensitivity (inset numbers) for different types of perturbations. Columns indicate the type of perturbation and rows indicate the type of target. For side wall study, the bottom width was kept constant at 25 nm. All the color scale bars should be multiplied by 10^{-3}. Seven trenches and nine holes were used for trench and hole targets, respectively.

Table 2. A summary of minimum sensitivities based on TSOM modeling along with their percentage sensitivities. λ = 520 nm

.		HT	SW	CD
DR32	Trenches in Si	0.25 nm	0.01°	0.02 nm
	%	0.03		0.08
	Holes in Oxide	0.2 nm	0.01°	0.07
	%	0.02		0.28
	Trenches in Oxide	0.2 nm	0.01°	0.08
	%	0.02		0.32
DR11	Trenches in Si	1.2 nm	0.01°	0.04 nm
	%	0.33		0.44
	Holes in Oxide	5 nm	0.02°	0.05 nm
	%	1.39		0.01
	Trenches in Oxide	1.5 nm	0.01°	0.1 nm
	%	0.42		1.11
Inf. Array	Trenches in Oxide	0.5 nm	0.05°	0.4 nm
	%	0.05		0.4

Optical simulations were also performed on a large array HAR trench grating targets shown in Fig. 4(a). The selected simulation conditions (Table 1) approximately match the experimental conditions shown later in the paper. For this type of target, 90˚ illumination polarization (e-field parallel to the trenches) showed higher sensitivity. For a 2 nm difference in the CD, 90˚ polarization resulted in an OIR of 5.0 compared to an OIR of 3.1 for 0˚ polarization. For this reason, 90° illumination polarization was used for all the subsequent simulations on this type of target. The sensitivity thresholds and D-TSOM patterns for different parametric variations are shown in Figs. 4(b) to 4(f). Two additional parametric variations were studied for this target relative to the smaller trenches: right sidewall only angle difference [Fig. 4(e)], and difference in the angle of the vertical axis [Fig. 4(f)]. These two types of variations resulted in asymmetric D-TSOM images. Unlike the finite number HAR features in Si oxide (Figs. 3 and 4), this target exhibits a different type of D-TSOM image patterns for CD and sidewall perturbations [Figs. 4(c) and 4(d)]. This indicates a possibility of differentiating CD and sidewall variations (i.e., the TSOM property 1 holds good). In general, this type of target shows less sensitivity compared to the 7-line finite gratings.

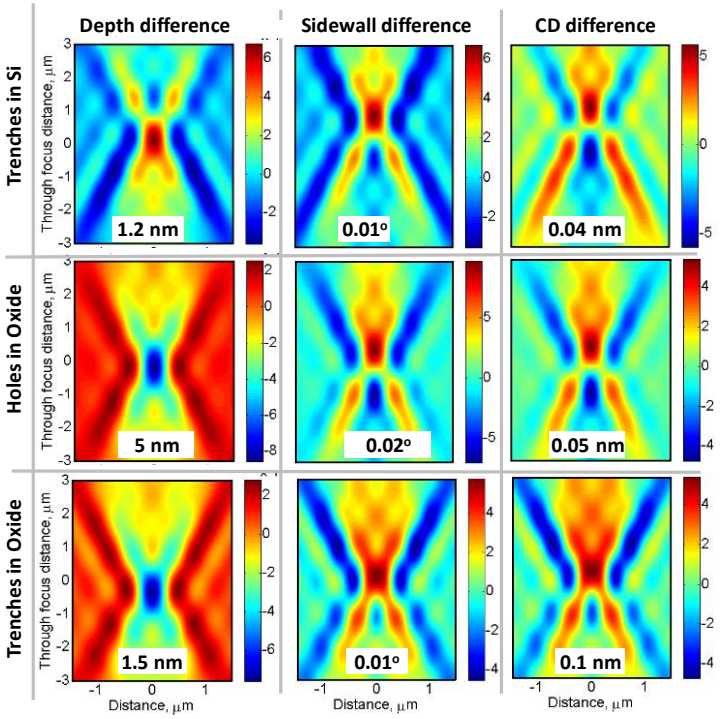

Fig. 3. Simulated D-TSOM images of 11 nm DR HAR trenches and holes showing minimum sensitivity (inset numbers) for different types of perturbations. Columns indicate the type of perturbation, and rows indicate the type of target. For side wall study, the bottom width was kept constant at 9 nm. All the color scale bars should be multiplied by 10^{-3}. Seven trenches and nine holes were used for trench and hole targets, respectively.

3.2 Experiments

A 300 mm wafer with HAR targets in a Si oxide layer was prepared [34] to perform TSOM metrology feasibility tests. The wafer had 1.1 µm Si oxide film on a Si substrate. HAR features were fabricated in the oxide film. Exposure and etch conditions were varied across the wafer. It is expected that variations in the feature structural parameters will exhibit a signature induced by processing conditions: a radial signature imparted by etch rate variations across the wafer, and a horizontal signature imposed by variation of lithography exposure conditions [Fig. 5(a)].

To study the effect of exposure and etch conditions, only the dies highlighted by crosshatches in Fig. 5(b) were analyzed in the current study. This provides horizontal and vertical signatures to compare with the expected signature resulting from fabrication conditions. A typical optical image is shown in Fig. 5(c). A typical etched HAR feature shows approximately 1.1 μm depth [Fig. 5(d)].

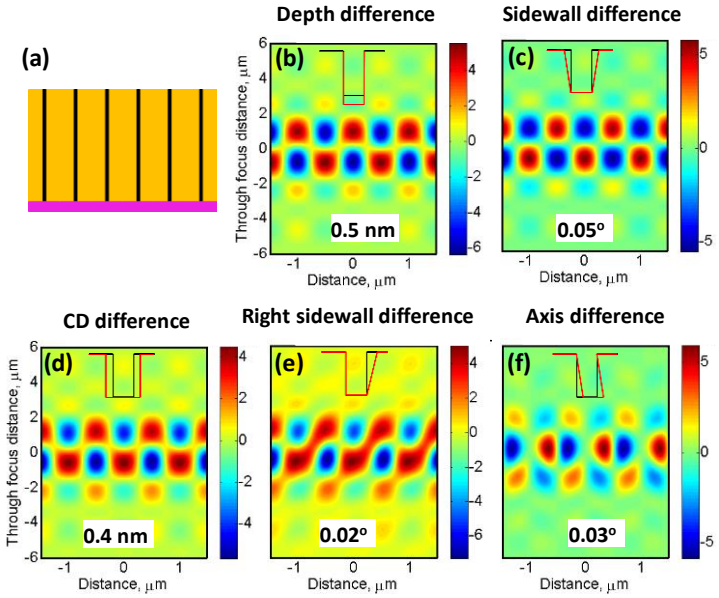

Fig. 4. (a) A schematic of the cross-sectional large-array HAR trenches in oxide layer used for the simulations. D-TSOM images for the perturbations of (b) depth, (c) sidewall, (d) CD, (e) right sidewall, and (f) axis that produce OIRs of just above 1. For side wall study, the bottom width was kept constant at 100 nm. In the inset images, the black and the red lines show the cross-sectional profiles of the reference and the perturbed targets, respectively. The inset numbers show representative minimum sensitivities for each parameter variation. All the color scale bars should be multiplied by 10^{-3}.

TSOM data were collected using a conventional, bright-field optical microscope in reflection mode. The microscope was designed for Kohler illumination. An LED lamp was used as an illumination source. A narrow, band-pass filter was used to obtain an illumination of 520 nm wavelength. High and low illumination numerical apertures (INA) of 0.75 and 0.25, respectively, were used in the current study, with a 0.75 collection NA objective. A through-focus step height of 300 nm and a total scan range of about 25 μm were used during the data acquisition. A cooled, monochrome CCD camera (692 x 520 pixels) was used to capture images. Other typical processing conditions used and the effect of optical parameters can be found in [31, 35]. The through-focus optical images forming the 3-D optical data set were analyzed using an in-house developed software program.

A test was conducted to determine the optimum polarization illumination. Similar to simulation results, it was found that 90˚ polarization showed higher sensitivity. For this reason, the subsequent experimental data were collected using 90˚ illumination polarization. A comparison of the TSOM results between 0.75 INA and 0.25 INA is presented in Fig. 6. The TSOM images [Figs. 6(a1) and (a2)] have distinctly different color patterns for the 0.25 and 0.75 INAs. However, the lower INA (low partial coherence factor) produces TSOM images with significantly stronger optical signals, as shown by the OIR values. In addition, the TSOM image at 0.25 INA has optical signal stretching through a larger focus range.

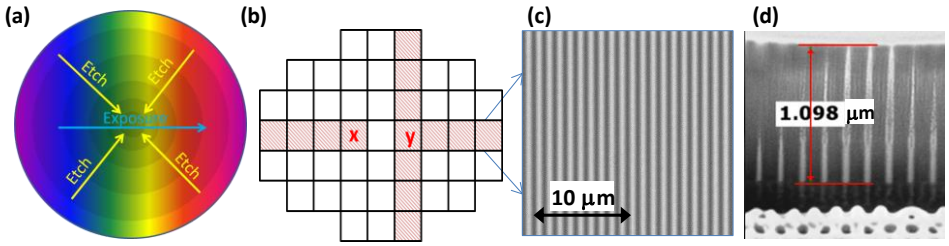

Fig. 5 (a) Exposure and etch conditions used to fabricate the HAR wafer. Exposure time increases from left to right. Etching changes radially, being slower at the edges. (b) Row and column dies selected for analysis are shown by cross hatches. Dies marked by 'x' and 'y' are the reference targets used for the left half and the right half of the wafer, respectively. The center die has a coordinate of (0,0). (c) A typical optical image of the selected HAR targets for analysis. CD = 100 nm, PT = 1000 nm, λ = 520 nm, INA = 0.11, CNA = 0.75. (d) Dual-beam, focused-ion-beam cross-sectional SEM images of HAR holes in oxide showing depth.

Different INAs produce distinctly different D-TSOM images using the same set of targets, as shown in column 2 [Fig. 6]. Similar to the TSOM images, the D-TSOM images show stronger signal (higher OIR) for the 0.25 INA. This demonstrates that TSOM shows higher sensitivity for HAR type of targets also at lower INAs (or at lower partial coherence factor [36]).

It is often thought that the optical images (or information) acquired outside the best focus range are not particularly useful. For this reason, much emphasis is given to determine the best focus and then to acquire images at this focus position. However, the D-TSOM image [Fig. 6(b2)] shows no differential signal around the best focus position, which is indicated by a dotted line. But it shows a strong differential pattern far away from the best focus position (on the lower half of the D-TSOM image). This useful differential signal is lost if the analysis is done near to the best focus position. TSOM facilitates accessing this type of useful optical signal beyond the best focus position.

The D-TSOM image shown in Figs. 6(c1) and 6(c2) again emphasize the importance of lower partial coherence factor. At the higher INA, the D-TSOM image appears noisy with no particular color pattern, implying no discernible dimensional difference between the two targets compared. However, at the lower INA, a clear color pattern with signal strength above the noise level can be observed. This clearly shows a discernible dimensional difference that only lower INA highlights [6].

Figs. 6(d1) and 6(d2) again show a stronger D-TSOM image pattern at the lower INA. However, at the higher INA, the D-TSOM image shows a discernible color pattern, even though its OIR of 0.79 is well below the noise level of one. This indicates a possibility of detecting dimensional differences even below the noise threshold level conservatively fixed in the current study at an OIR of one. It also suggests that the noise threshold level criteria could be lowered.

Since the results shown above clearly demonstrate superior performance of the lower INA, only the results using 0.25 INA are presented in the following section.

A summary of TSOM image analysis performed along the horizontal and vertical directions [Fig. 5(b)] is presented in Fig. 7. On the left half of the wafer, both exposure and etch rate increased from left to right. D-TSOM image patterns on this part of the wafer show low OIR values (red line). Similarly, not much variation in the OIR values can be observed. However, D-TSOM image patterns change indicating different types of dimensional differences. Low OIR values could also mean lower magnitude differences in dimension (TSOM property 3). On the right half of the wafer, exposure increased but etch rate decreased from left to right. This combination produced similar D-TSOM images. This may indicate changes in similar target dimensions on dies in this row. However, their OIR values increased

drastically from left to right, indicating that the difference in the magnitude increased from left to right on the right half.

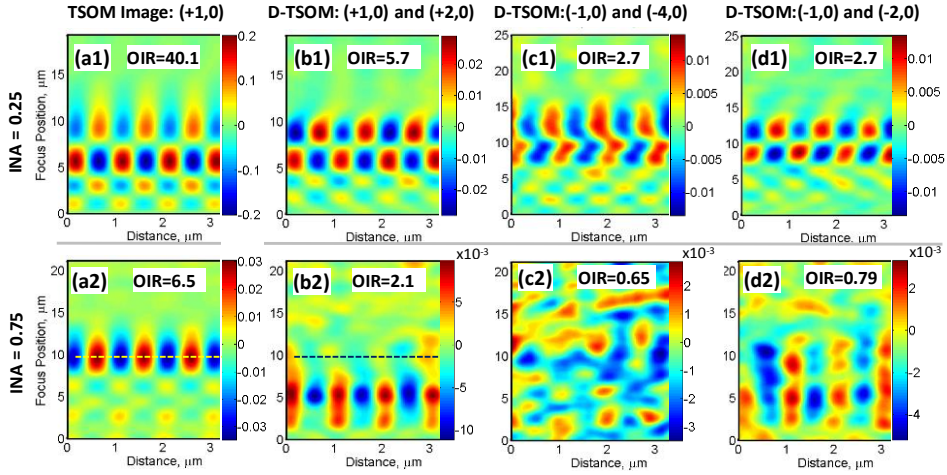

Fig. 6 Experimentally obtained TSOM images at (a1) 0.25 and (a2) 0.75 INAs for the die indicated at the top. (b1,b2,c1,c2,d1,d2): D-TSOM images between the dies indicated at the top. Dotted lines in columns 1 and 2 (second row) indicate location of the best focus position. The OIR values indicated are the mean of at least five repeats and have standard deviations of less than 7 %. Nominal CD = 100 nm, nominal pitch = 1000 nm, l = 520 nm, collection numerical aperture (CNA) = 0.75.

From top to bottom exposure is the same, however, etch rate decreased radially. These conditions produced D-TSOM images with varying color patterns indicating different types or combinations of dimensional differences. In general, OIR values are lower in the middle of the wafer and increase toward the edges of the wafer. This shows that dimensional differences increase in magnitude towards the edges of the wafer (compared with the reference target at 'y' [Fig. 5(b))].

Some useful inferences can be made if a comparison is performed between the experimental D-TSOM image results [Fig. 7] and that of the simulated result [Fig. 4]. Simulations show that purely CD, (symmetric) sidewall, and trench depth or any combination of these parameters will result in D-TSOM images that are symmetric about the vertical (focus direction) axis [Figs.4 (b) to 4(d)]. This could indicate that on the right side of the experimental wafer [Fig. 7], variances are mostly dominated by these three types of differences producing symmetrical D-TSOM images along the focus direction. However, when sidewall asymmetry or axial asymmetry is introduced in the simulations, the D-TSOM image exhibits vertical asymmetry. This shows that the dimensional differences in the vertical direction of the wafer [Fig. 7] are dominated by asymmetrical differences in the HAR targets. This asymmetry appears to increase towards the edges. On the far left side of the wafer, again differences appear to be dominated by asymmetries. Towards the center on the left side, the domination of asymmetry reduced.

In summary, the D-TSOM image patterns and the OIR values were found to vary radially both in the vertical and horizontal directions, approximately matching the fabrication conditions and expected signature. These results demonstrate that TSOM can identify process variations across the wafer. Based on the simulation results presented above, it may be hard to distinguish purely CD and sidewall angle differences for small DR finite array HAR features in the Si oxide layer. Simulations on large gratings indicate that the CD and sidewall could be differentiated in this case. At this time, it has not yet been determined by an independent method which parameter variations are present in the wafer that was analyzed. Further characterization using tools such as focused ion beam, transmission electron microscopy, and atomic force microscopy

is currently underway and will allow for the establishment of a correlation between OIR, D-TSOM, and variation of the structural parameters of the trenches.

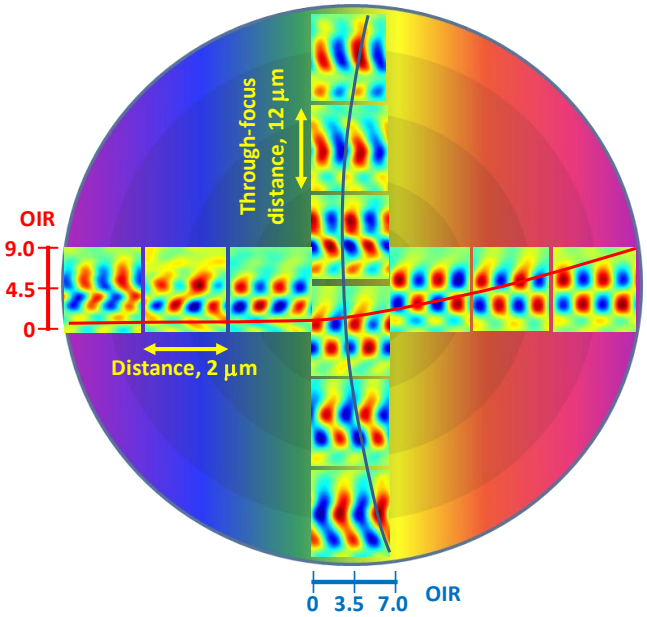

Fig. 7 Measured D-TSOM images approximately positioned at their respective locations on the wafer. Red (horizontal) and blue (vertical) curves show general trends in the OIR values in their respective directions and also represent their color scale range. INA=0.25

TSOM has an inherent advantage over conventional optical imaging as it collects substantially more 3-D optical information [25]. It is also capable of analyzing isolated targets (as compared to scatterometry). This enables TSOM to simultaneously analyze several targets or locations present in the optical field-of-view. In addition, substantially smaller grating targets are sufficient for the TSOM metrology analysis, compared to the conventional 30 µm to 50 µm square grating targets required for scatterometry analysis. The width of the grating targets used in the current study did not exceed 0.5 µm. To minimize the optical interference from the ends of the line, the optimal length of the grating needed for TSOM analysis is about 10 times the wavelength, i.e., about 5 µm. Similarly, to minimize optical interference, it is best to have a free space of about five times the wavelength on both sides of the target HAR features, i.e., about 2.5 µm on each side. This results in an optimal target area that is over 50 times smaller than a typical scatterometry target. The target area required for a lower wavelength such as 250 nm can be even smaller (over 100 times smaller). This potentially results in cost savings by considerably reducing the real estate required for metrology targets. This may also improve measurement accuracy by enabling the metrology targets to be placed in the active area of the wafer (due to smaller areas needed). In addition, the present work demonstrates that TSOM can be implemented using widely available, visible-wavelength, conventional optical microscopes. This is an attractive metrology solution since it can easily be built, it is low-cost, and it has a relatively high through-put. In comparison to the other semiconductor metrology tools, the TSOM measurement time was considered "excellent", on par with scatterometry [3]. Under the optimized conditions the TSOM measurement time can be significantly less than 200 ms [35,37], making it an attractive solution for high volume manufacturing. In addition, several

targets located in a given field-of-view can be analyzed simultaneously from a single set of through-focus data.

4. Conclusions

In this work we evaluated the possibility of using TSOM to detect 3-D shape variations present in HAR features by making use of the three properties of D-TSOM images. We performed both simulations and measurements using visible wavelength illumination. Simulations demonstrated the ability of TSOM to detect nanoscale 3-D shape variations of HAR targets. Sensitivity to sidewall angle of HAR features appears to be a strong capability of TSOM. Simulated sensitivity obtained by TSOM either matches or exceeds ITRS requirements down to the 11 nm node. Experimental TSOM result trends correlate with the expected variations based on the fabrication conditions of the wafer. At this time, some broad inferences regarding the shape of the HAR targets could be made based on the symmetries of the D-TSOM images. TSOM might make an effective hybrid pairing with LL-BSE CD-SEM [33] for accurate HAR measurements—the authors hope to see this further explored. These results suggest TSOM has the potential to provide an economical additional capability for process control and yield enhancement in high volume manufacturing, if throughput can be kept compatible with ITRS requirements for bright field inspection (≈1000 cm^2/hr).

Acknowledgments

Yuki Chiba, Timothy Gilday, and Akiteru Ko from Tokyo Electron were very helpful in performing the HAR etch, and James Nadeau of FEI performed the cross-section of these features. The authors also thank Hyeong-Gon Kang for miscellaneous help and the Summer Undergraduate Research Fellowship (SURF) program of NIST and NSF for providing an internship to Peter Weck.

Disclaimer: Certain commercial materials and equipment are identified in order to adequately specify the experimental procedure. Such identification does not imply recommendation by the National Institute of Standards and Technology (NIST) or by SUNY Polytechnic SEMATECH.